
LTAU-FF: Loss Trajectory Analysis for Uncertainty in Atomistic Force Fields

Joshua A. Vita

Materials Science Division
Lawrence Livermore National Laboratory
Livermore, California 94550, USA

Amit Samanta

Physics Division
Lawrence Livermore National Laboratory
Livermore, California 94550, USA

Fei Zhou

Physics Division
Lawrence Livermore National Laboratory
Livermore, California 94550, USA

Vincenzo Lordi

Materials Science Division
Lawrence Livermore National Laboratory
Livermore, California 94550, USA

Abstract

Model ensembles are effective tools for estimating prediction uncertainty in deep learning atomistic force fields. However, their widespread adoption is hindered by high computational costs and overconfident error estimates. In this work, we address these challenges by leveraging distributions of per-sample errors obtained during training and employing a distance-based similarity search in the model latent space. Our method, which we call LTAU, efficiently estimates the full probability distribution function (PDF) of errors for any test point using the logged training errors, achieving speeds that are 2–3 orders of magnitudes faster than typical ensemble methods and allowing it to be used for tasks where training or evaluating multiple models would be infeasible. We apply LTAU towards estimating parametric uncertainty in atomistic force fields (LTAU-FF), demonstrating that its improved ensemble diversity produces well-calibrated confidence intervals and predicts errors that correlate strongly with the true errors for data near the training domain. Furthermore, we show that the errors predicted by LTAU-FF can be used in practical applications for detecting out-of-domain data, tuning model performance, and predicting failure during simulations. We believe that LTAU will be a valuable tool for uncertainty quantification (UQ) in atomistic force fields and is a promising method that should be further explored in other domains of machine learning.

1 Introduction

In computational chemistry and materials science, deep learning force fields have become an established tool for accelerating quantum mechanical calculations [1, 2, 3]. The goal of these force fields is to perform the regression task of reproducing the potential energy surface of systems containing hundreds to millions or billions of atoms of one or more elemental types in a computationally efficient way [4, 5]. This is done by learning to predict the energies and atomic forces from a high-accuracy ground truth, such as density functional theory (DFT). A number of different approaches to this problem have been developed over the years, including the use of Gaussian processes [6, 7], symbolic regression [8], feed-forward neural networks [9, 10], and message-passing neural networks [11, 12], among others.

While multiple UQ techniques have been applied to atomistic force fields, including dropout neural networks [13], Bayesian frameworks [14, 15], or Gaussian mixture models [16], by far the most popular approach in practice is the use of ensemble-based methods, where the ensemble variance

is taken as a measure of the predictive uncertainty of the model. Particularly beneficial is the fact that these ensemble methods do not require any modifications to the model architecture or training algorithm, and therefore can be readily applied to any existing development workflow. Due in large part to this simplicity and generalizability, ensemble-based UQ techniques have been widely applied towards estimating parametric uncertainty in numerous machine learning and deep learning tasks [17, 18], and are often considered to be the gold standard when evaluating the performance of new UQ methods for atomistic force fields [19, 20, 21, 22, 16, 23].

Despite their ubiquity, ensemble methods typically suffer from two main drawbacks: high computational costs (for both training and inference) and difficulties maintaining ensemble diversity that result in overconfident uncertainty estimates. In particular, ensemble sizes of approximately 5 to 30 models have been found to be necessary for various practical applications of UQ for force fields [24, 25], making ensemble-based methods potentially infeasible for large training sets or expensive models. Furthermore, although ensemble-based UQ techniques have been shown to typically outperform single-model methods [26], there is growing evidence that they result in overconfident UQ measures [27, 25, 28, 29, 18], which is attributed to a lack of ensemble diversity. Intuitively, the most straightforward approaches to ensemble generation (training multiple models with different initial weights, data splits, or training hyperparameters [30]) will only sample models at different local minima of the loss function. These methods therefore fail to account for the full topography of the loss surface, which has been shown in many cases to be important for minimizing generalization error [31, 32, 33, 34, 35, 36] and to be valuable for estimating model uncertainty and detecting out-of-domain data [28, 37].

In this work, we develop the new LTAU method, which is an ensemble-based technique that addresses the issues of computational cost and ensemble diversity, and can be broadly applied to any model architecture. Specifically, we provide the following contributions:

- We outline our proposed method, LTAU, which utilizes the PDF of errors sampled during training to provide confidence intervals and expected error estimates for any prediction made with the model. This use of the training error trajectories imposes no additional computational overhead during training and improves the diversity of the ensemble by incorporating additional information from various points on the loss landscape.
- Coupling the training PDFs to a nearest-neighbor search in the model’s latent space, we show how LTAU can provide a cheap, easy-to-implement UQ measure that does not require training or evaluating multiple models. We apply LTAU to atomistic force fields (LTAU–FF), where we observe that it is 2–3 orders of magnitude faster than typical ensemble techniques.
- We quantitatively assess the robustness of LTAU–FF, showing that it produces well-calibrated confidence intervals and predicts errors that correlate strongly with the true errors for data near the training domain. Furthermore, we observe that by using thresholds on the distance metric in the latent space, it is possible to identify out-of-domain data for which the predictions made by LTAU–FF may be less accurate.
- Finally, to demonstrate the utility of LTAU–FF in practical applications, we conduct two experiments: 1) re-weighting the training set of the model to prioritize high or low uncertainty samples, and 2) applying our method to the IS2RS task from the OC20 challenge (where it is infeasible to train multiple models) to predict errors in relaxation trajectories.

2 Background

The defining trait of the LTAU method developed in this work, which distinguishes it from other ensemble-based UQ methods, is its ability to leverage information from large ensembles of models while only having to evaluate a single model during inference. This is achieved through efficient use of logged error trajectories sampled during training and a similarity search in the model’s latent space during inference. The method builds heavily upon two key concepts in deep learning: training trajectory analysis and distance-based UQ, which are discussed further in this section.

2.1 Training trajectory analysis

Training trajectories have been used in a number of deep learning applications for the purpose of outlier detection [38, 39, 40, 41, 42], data pruning [43, 44, 45, 46, 47, 42], and influence estimation

[48, 49, 50]. These approaches have leveraged the rich information that is sampled over the course of training, including loss gradients [51, 45, 46, 44, 41, 44, 40], Softmax outputs [38, 52], or other custom metrics [39, 43, 49, 42]. However, many of these metrics have been designed primarily for classification tasks (i.e., they are derived using assumptions about the loss function or model architecture that are unique to classification) and require modification in order to be applied in regression settings. In this work we show that the distribution of errors sampled during training can serve as a useful extension of these trajectory analysis techniques to regression tasks for estimating parametric uncertainty and detecting out-of-domain samples.

2.2 Distance-based UQ

A critical assumption of the method developed in this work is that points which are close to each other in the model’s latent space also have similar error PDFs. On a smoothly-varying manifold, proximity between points is often used to infer or model function values. This notion has been successfully applied to develop tools like radial basis functions, Gaussian process regression, and many others. Similarly, this concept has been applied to UQ, where a simple method for estimating the uncertainty in a model’s prediction for a test point is to use the weighted Euclidean distance (in either the input space or a latent space) between the test point and the nearest training point [53, 54, 47].

While related methods have been used for UQ with atomistic force fields [55, 56, 16], a distance metric alone is insufficient for constructing well-calibrated uncertainty estimates, and usually requires additional calibration techniques or making assumptions regarding the distribution of errors [57]. Specifically, any distance-based UQ metric would be expected to fail in the case where a point is far enough from any other point that the assumption of local smoothness of the model uncertainty does not hold. This issue is discussed further in Section 4.1, where we find that the confidence intervals and expected errors predicted by LTAU-FF become less accurate when used on out-of-domain (OOD) data. This issue is not unique to our method, and emphasizes the importance of coupling UQ metrics with suitable tools for detecting OOD data.

3 Methods

3.1 Model

We use the NequIP model [11] as the deep learning force field in this work. NequIP is a graph-based message-passing neural network that uses spherical harmonics to represent local atomic environments with equivariant features. The use of message-passing and an equivariant architecture, respectively, have been shown to be useful for incorporating long-range interactions in the model and avoiding issues caused by the inability of invariant models to distinguish between symmetrically-equivalent atomic environments [58]. Because of this, NequIP (alongside other equivariant message-passing models) has achieved state-of-the-art performance for a number of applications [59, 60]. The hyperparameters of the model are adjusted for each dataset, with details provided in Appendix B.

3.2 Datasets

Three training datasets are used in this work: 3BPA [61], Carbon_GAP_20 [62], and the 200k split of the S2EF task from the OC20 challenge [63]. These datasets were chosen deliberately to provide systematic tests of the limitations of our method with increasingly complex data. We start with a simple molecular test case for refining our method (3BPA), then expand to a more diverse dataset typical of solid-state force field fitting tasks (Carbon_GAP_20), and finally test against a challenging real-world application (IS2RS task from OC20) that is intractable using typical ensemble methods. Detailed descriptions of the datasets are found in Appendix C and the referenced citations. All datasets are publicly available from their original sources.

3.3 Training details

For the most part, standard published hyperparameters and techniques were used for training the NequIP models in this work, with details provided in Appendix B. As a notable exception, for all analysis shown in this work for the 3BPA and Carbon_GAP_20 datasets we trained the models **only to forces**, which is in contrast to typical force field fitting workflows that usually also include an

energy term in the loss function. We chose to weight the energy contributions to 0.0 in these cases for two reasons: 1) because a system’s energy cannot be uniquely decomposed into a per-atom quantity, thus making it a less suitable target for constructing a per-atom UQ metric; and 2) because a trade-off is commonly observed in practice between the energy and force terms in the loss function, raising concerns that training to energies could interfere with our analysis. Training only to forces for the 3BPA and Carbon_GAP_20 datasets thus allowed us to obtain a clearer understanding of the performance of our method. For the OC20 dataset, we weighted the energy term to 1.0 (and the force term to 100.0) to help avoid unexpected behavior during energy minimization; we note that this still resulted in strong correlation between the UQ metric provided by LTAU-FF and the accuracy of the predicted ground-state structure, as shown in Section 4.2.

3.4 LTAU-FF

As the primary contribution of this paper, we propose the **Loss Trajectory Analysis for Uncertainty** (LTAU) method (Algorithm 1 and Algorithm 2), and demonstrate its application to atomistic force fields (LTAU-FF: LTAU for atomistic **F**orce **F**ields). The LTAU method builds upon the concepts described in Section 1, using the distributions of errors observed by the ensemble of models sampled during training to approximate the PDFs of all training points. The training error PDFs are then coupled to a distance-based similarity search for estimating the PDFs for test predictions. Implementing LTAU in an existing workflow will typically only require patching the training code to log per-sample errors at every epoch and adding some basic post-processing steps. We provide code and utility functions for performing this postprocessing and working with the models presented in this work, which will be released upon completion of the peer review of this article.

For LTAU-FF, the first step to computing the uncertainty in this manner is to train a model and log the errors at every epoch (Algorithm 1). By logging the model’s errors on every sample (i.e., every atom) at every epoch, we can construct error trajectories $T_i = \{\epsilon_i^1, \dots, \epsilon_i^E\}$ for every atom i , where $\epsilon_i^t = \|\mathbf{F}_{i,DFT} - \mathbf{F}_i^t\|_2$ is the L_2 norm of the force error vector between the true ($\mathbf{F}_{i,DFT}$) and predicted (\mathbf{F}_i^t) forces for atom i at the end of epoch t , and E is the total number of training epochs. Alternative error metrics can also be used instead of the L_2 norm – for example, the mass-normalized errors explored in [64] would be particularly useful for multi-element systems.

Algorithm 1: Compute PDFs and descriptors of training points

Input : Model, \mathcal{F} ; training set \mathcal{S} of size N ; epochs, E ; bin edges, $bins$

Output : PDFs of training points, $p = \{\text{PDF}_1, \dots, \text{PDF}_N\}$; descriptors of training points, D

```

1 for  $e = 1 \dots E$  do
2   |   Train( $\mathcal{F}$ )
3   |   Log(Error( $\mathcal{F}$ ,  $\mathcal{S}$ ),  $e$ )
4 end
5  $T \leftarrow$  LoadErrorTrajectories()
6  $p \leftarrow$  Histograms( $T$ ,  $bins$ )
7  $D \leftarrow$  Descriptors( $\mathcal{F}$ ,  $\mathcal{S}$ )
8 return  $p$ ,  $D$ 
```

Algorithm 2: Estimate PDF of test point

Input : Model, \mathcal{F} ; training PDFs, p ; training descriptors, D ; test point, x_j ; number of nearest neighbors, k

Output : Estimated PDF of test point, p_j

```

1  $d_j \leftarrow$  Descriptor( $\mathcal{F}$ ,  $x_j$ )
2  $\mathcal{N}_j \leftarrow$  NearestNeighbors( $d_j$ ,  $D$ ,  $k$ )
3 return  $\frac{1}{k} \sum_{i \in \mathcal{N}_j} p_i$ 
```

Once training is complete, as a post-processing step we can compute the error PDFs, p_i , for each atom i by loading the array of logged error trajectories, then binning the observed errors into a chosen set of bins. Though a maximum error value, ϵ_{max} , defining the upper edge of the uppermost bin may not necessarily be known *a priori*, there are many reasonable choices that could be made without any knowledge of the expected test errors. For example, ϵ_{max} could be set to be a multiple of the maximum error observed during training, or the maximum “acceptable” error as determined by the application of interest. In Section 4.1, we chose to set ϵ_{max} to be the maximum error observed during training. To use the PDFs computed on the training set for predicting the PDF of a test point, j , we compute $p_j = \frac{1}{k} \sum_{i \in \mathcal{N}_j} p_i$ by averaging the value in each bin over \mathcal{N}_j , the k nearest samples of j

from the training set (Algorithm 2). In practice, we observed that LTAU was relatively insensitive to the choice of k , so we chose to use $k = 10$ for all experiments.

The k nearest neighbors are obtained by performing a similarity search in the latent space of the model. Specifically, using the output of the last message-passing layer of the NequIP model (prior to the linear readout layers) as the atomic descriptor, as is done elsewhere in the literature [16]. This means that we must evaluate the model for the full training set, store the latent descriptors for all training atoms, then compare the descriptors for each test atom, j . The cost of computing p_j then necessarily scales with the size of the training set, the number of neighbors k , and the dimensionality of the latent space (which was 32 for all experiments in this work). Note that the latent descriptors will already be computed when performing a forward pass of the model, so p_j can be efficiently estimated with only a minor increase in cost compared to a force evaluation, as shown in Section 4.3.

Since typical training sets for force fields can include $\mathcal{O}(10^4)$ - $\mathcal{O}(10^7)$ atoms, we rely upon the FAISS [65] package for efficiently searching for the k nearest neighbors of test points. In the case of the the Carbon_GAP_20 and OC20 datasets, where the training sets were particularly large, we used the IndexHNSWFlat algorithm provided by FAISS. IndexHNSWFlat is an *approximate* nearest neighbor search that scales well to large datasets while maintaining good accuracy. For the 3BPA dataset, an exact brute-force algorithm was used. Additional details regarding the FAISS hyperparameters used in this work can be found in Appendix B.

4 Results and Discussion

4.1 Comparisons to an ensemble-based method

As an initial comparison between LTAU-FF and a typical ensemble method (henceforth referred to as Ensemble), we train an ensemble of 10 models to the 3BPA and Carbon_GAP_20 datasets, then compare the quality of the uncertainty estimates provided by each method on the test sets.

In Fig. 1a and Fig. 2a we plot the per-atom force uncertainties versus the true force errors observed on the test sets (averaged over the ensemble). The uncertainty predicted by LTAU-FF for atom i is obtained by taking the expectation value of p_i (the PDF of errors for atom i). As is typically done in the literature [19, 20, 21, 22, 16, 23], for the uncertainty predicted by Ensemble we use the standard deviation of the ensemble’s force predictions averaged over the Cartesian directions. Note that the uncertainty metric provided by LTAU-FF can be directly interpreted as an error estimate, whereas those obtained from Ensemble cannot since they simply correspond to the spread in predictions by different models in the ensemble.

To generate the calibration curves shown in Fig. 1b and Fig. 2b, we compute the fraction of points whose true errors fall within confidence intervals ranging from 0% to 100% for each method. The calibration curves can thus be thought of as a comparison between the true and predicted CDF of the test errors, where a well-calibrated model would have a calibration curve that falls close to the $x = y$ line [66]. For Ensemble, the error thresholds corresponding to a given confidence interval can be obtained by assuming that the errors of each atom follow a Gaussian distribution with variance equal to the ensemble variance of the force predictions for that atom, then computing the z-score at the desired confidence level. For LTAU-FF, since the CDFs can be directly computed from the predicted PDFs, the error thresholds can be determined by finding the bin edge at which the CDF first reaches the desired confidence level.

Table 1 provides a quantitative analysis of Fig. 1 and Fig. 2. The Pearson (C_P) and Spearman (C_S) coefficients are used to measure the correlation between the uncertainty estimates and the true errors. We quantify the degree of miscalibration by computing the area ($|\mathcal{A}|$) between the calibration curves and the ideal $x = y$ line, as is done in [66]. To provide additional analysis, we further decompose the miscalibration area into the area below/above the $x = y$ line (\mathcal{A}^+ and \mathcal{A}^- , denoting the degree of *overconfidence* and *underconfidence* of the method, respectively). Finally, the “sharpness” [66] is calculated by computing the variance of each atom’s predicted error distribution, averaging over all atoms in the test set, then taking the square root (to recover the original units of eV/Å). An ideal UQ method would have uncertainty estimates which strongly correlate with the true errors (high C_P and/or C_S) and have confidence intervals which are as small as possible (low s) while still capturing the true errors (low \mathcal{A}^+ , \mathcal{A}^- , and $|\mathcal{A}|$). For the LTAU-FF results in Table 1, the metrics are computed for each model in the ensemble individually, then averaged over the ensemble. The variance in the

metrics for LTAU-FF was negligible (less than 0.01 in all cases). For Ensemble, the uncertainty measure is the same for all models in the ensemble, so no averaging is possible.

3BPA

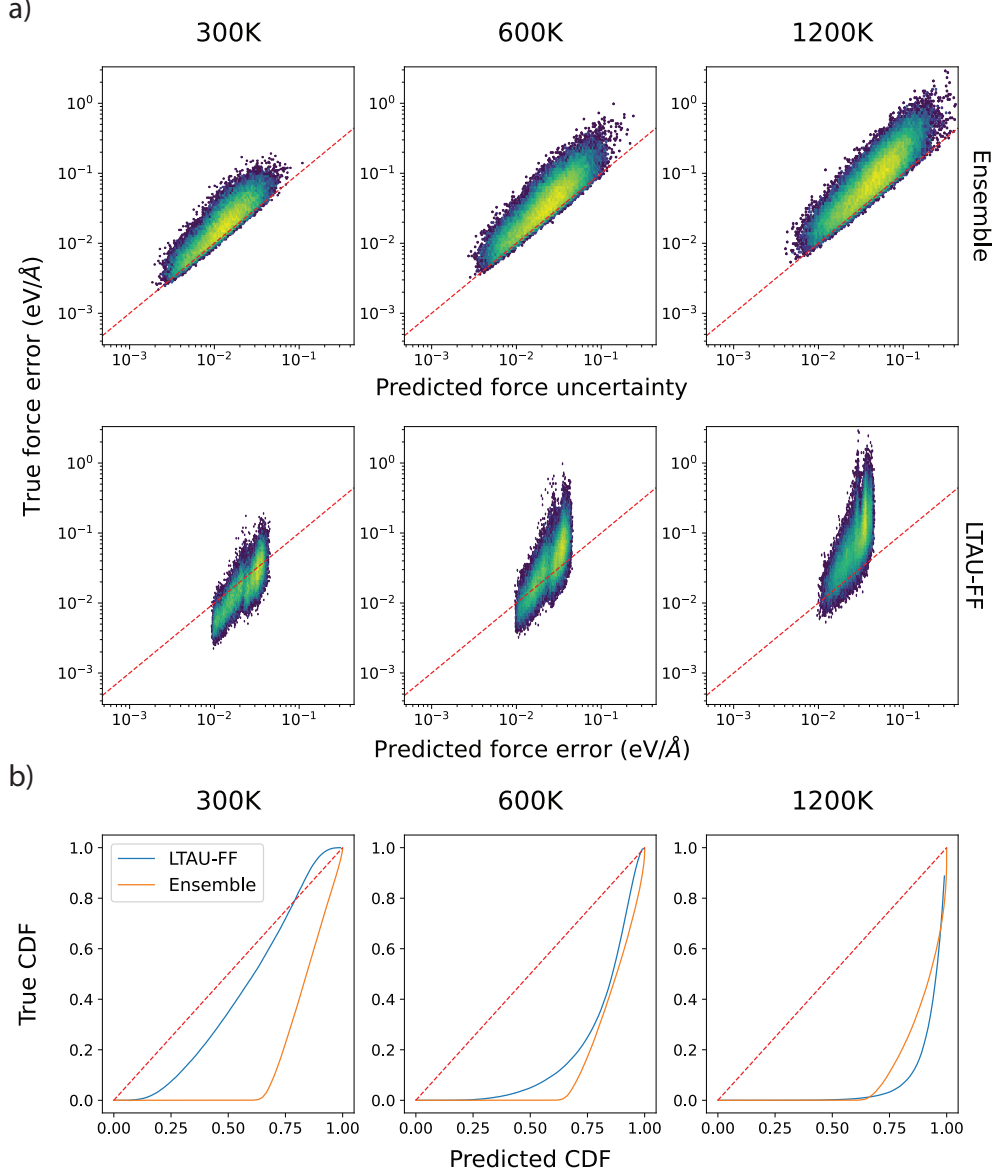


Figure 1: Comparison of LTAU-FF and Ensemble on the the 3BPA test sets. Panel a compares the uncertainty estimates for each method to the true errors observed on the test sets (note the log-scaled axes), and can be used to obtain \mathcal{C}_P and \mathcal{C}_S in Table 1. The calibration curves, as described in [66], show how well the predicted confidence intervals capture the true errors (with an ideal model falling on the $x = y$ line), and can be used to obtain \mathcal{A}^+ , \mathcal{A}^- , $|\mathcal{A}|$, and s in Table 1.

Before analyzing the results in Fig. 1 and Table 1, it is important to recall some of the main features and limitations of LTAU-FF. First, because LTAU-FF is also an ensemble method, we can expect that it should perform similarly to Ensemble, though with the additional benefit of having more conservative uncertainty estimates due to the increased diversity of the ensemble sampled during training. Second, since LTAU-FF relies upon a distance-based similarity search for estimating the

PDFs of errors for test points, it can be expected to suffer from the drawbacks described in Section 2.2, leading to decreased performance when the test data are far from the training set.

Considering first only the 300K data, it can be seen that LTAU-FF outperforms Ensemble for the in-domain (ID) data. Both methods have reasonably good \mathcal{C}_P and \mathcal{C}_S coefficients, but LTAU-FF has an $|\mathcal{A}|$ area that is $3\times$ lower and a sharpness that is $2\times$ lower than those of Ensemble. This is consistent with our expectations that the increased diversity of the training ensemble would help address the documented overconfidence issues of Ensemble [27, 25].

However, when moving to the higher-temperature (600K and 1200K) data, we observe decreased performance from LTAU-FF quantified by lower correlation coefficients and higher miscalibration areas. We hypothesize that this is caused by the fact that the nearest-neighbor search used by LTAU-FF is unable to account for the effects of increasing distance in the latent space when predicting the PDF of errors for test points. For example, even if one of the k nearest-neighbors is significantly further away from a test point j than another of the k nearest-neighbors, it will still have an equal influence on the uncertainty estimate. This deficiency is one of the most important weaknesses of LTAU-FF.

We propose a possible solution to this issue in the next section using distance thresholds to detect out-of-domain (OOD) data; however, we emphasize that further improvements are still necessary. Modifying LTAU-FF to improve its performance on OOD or “near OOD” data (that which is OOD, but with distributions similar to the training data) [67], for example by weighting the neighbor average based on neighbor distance or coupling it to additional OOD-detection algorithms, would greatly improve the method. Furthermore, it is worth noting that both Ensemble and LTAU-FF, like most UQ metrics, would benefit from additional re-calibration techniques such as the use of an external “calibration set” [68]. Especially considering the high \mathcal{C}_P coefficients, even a simple linear transformation of the uncertainty estimates would likely greatly improve the calibrations of both methods. Nevertheless, the good calibration of LTAU-FF on ID data *without* requiring additional calibration is a notable strength of the method.

Carbon_GAP_20

The results on the Carbon_GAP_20 dataset shown in Fig. 2 reinforce the conclusions drawn from the 3BPA results: that LTAU-FF outperforms Ensemble on ID data and is generally the better calibrated metric, but may struggle to estimate errors for OOD data. Most notably, the results for LTAU-FF in Fig. 2a appear to hit a “wall” where the method does not predict errors larger than approximately 1 eV/Å. A similar effect can be seen for the 3BPA results in Fig. 1a around 0.05 eV/Å.

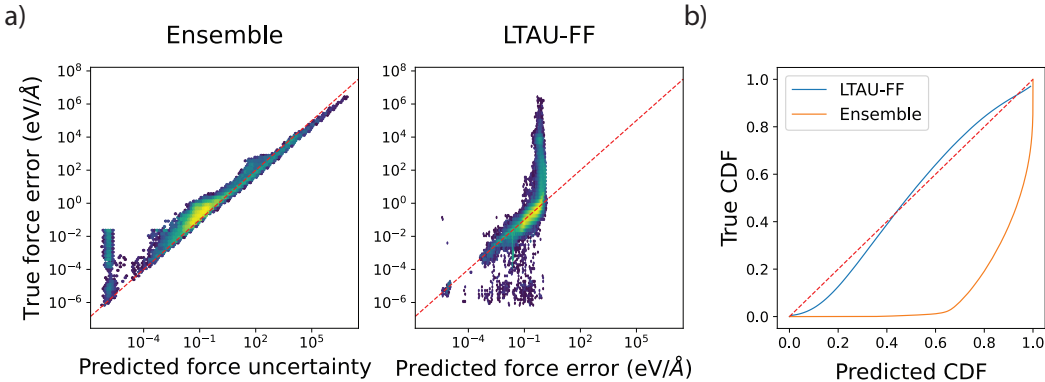


Figure 2: Comparison of LTAU-FF and Ensemble on the Carbon_GAP_20 test set. Predicted uncertainty vs. true force errors shown in panel **a** and calibration curves in panel **b** are as described in Fig. 1. Quantitative analysis is provided in Table 1. The “wall” of points around 1 eV/Å where LTAU-FF makes poor predictions are those which we identify as being OOD based on their nearest-neighbor distance in the latent space (see Appendix D).

While this effect is in part due to the fact that the errors observed during training may be significantly smaller than those observed on the test sets, the issue can be best understood by analyzing the distributions of nearest-neighbor distances in Fig. D1. It can be seen that for both datasets there are a small number of points in the training data which have a significantly larger first nearest-neighbor

distance than the rest of the training set. By choosing a distance cutoff close to the lower bound of these higher distances, we can define a point as being ID if it has a nearest neighbor distance below the cutoff, or OOD otherwise. We observe in Fig. D2 and Fig. D3 that the “walls” in Fig. 1 and Fig. 2 roughly correspond to the data which are identified as being OOD based on the distance cutoffs. This observation suggests a possible avenue forward for improving LTAU-FF to warn when the method may be unreliable on OOD data, thus hopefully addressing the main limitation of this work.

Table 1: Metrics for comparing UQ methods. \mathcal{C}_P and \mathcal{C}_S are the Pearson and Spearman correlation coefficients; \mathcal{A}^+ , \mathcal{A}^- , and $|\mathcal{A}|$ provide measures of the degree of miscalibration [66] (overconfidence, underconfidence, and total, respectively); s is the “sharpness,” [66] which measures how narrow the confidence intervals are (in the same units as the model predictions). Arrows (\uparrow , \downarrow) denote if larger or smaller values are better, respectively. The near-zero \mathcal{C}_P score of LTAU-FF on the Carbon_GAP_20 dataset is caused by the “wall” in Fig. 2.

Test set	Method	$\mathcal{C}_P(\uparrow)$	$\mathcal{C}_S(\uparrow)$	$\mathcal{A}^+(\downarrow)$	$\mathcal{A}^-(\downarrow)$	$ \mathcal{A} (\downarrow)$	$s(\downarrow, \text{eV}/\text{\AA})$
3BPA (300K)	Ensemble	0.83	0.90	0.34	0.0	0.34	0.12
	LTAU-FF	0.73	0.84	0.10	0.01	0.11	0.06
3BPA (600K)	Ensemble	0.81	0.89	0.36	0.0	0.36	0.16
	LTAU-FF	0.63	0.82	0.31	0.0	0.31	0.07
3BPA (1200K)	Ensemble	0.80	0.89	0.40	0.0	0.40	0.23
	LTAU-FF	0.54	0.77	0.43	0.0	0.43	0.08
Carbon_GAP_20	Ensemble	0.99	0.87	0.40	0.0	0.40	12.11
	LTAU-FF	0.02	0.91	0.02	0.02	0.04	0.29

4.2 Applications

Tuning the training–validation gap

As an initial application of our method, we test if the uncertainty estimates provided by LTAU-FF can be used to tune the training-validation gap on the Carbon_GAP_20 dataset. Fig. E1 shows that by increasing the weight of high-uncertainty samples it is possible to decrease the training error (while correspondingly increasing the validation error). Conversely, by increasing the weight of the low-uncertainty samples, it is possible to *decrease* the training-validation gap, which would be expected to result in a more generalizable model. We further confirmed the performance gaps by computing the ensemble test errors for each weighting scheme, as shown in Fig. E2 where increasing the weight on low-uncertainty points decreased the errors on outlying test points by an order of magnitude. Additional details for this experiment are provided in Appendix E.

These results are consistent with literature from other fields of deep learning where it has been shown that measures of sample difficulty may be valuable for tuning model performance. For example, Feldman et al. [48, 49] hypothesized that difficult (high uncertainty) samples are essential for fitting to datasets with long-tailed distributions, which is supported by our observation that increasing the weight of high-uncertainty samples leads to increasing degrees of overfitting. This connection to the literature implies many possible applications of LTAU-FF that build upon the work by Feldman et al. for dataset pruning and active learning, where it has been shown that sample difficulty metrics and training trajectory analysis can be used for constructing optimal training sets [43, 38, 41, 47]

Leveraging the UQ metric during simulations

The final test of LTAU-FF that we performed was to train a model to the 200k split of the OC20 S2EF task, then to see if LTAU-FF could predict model performance on the IS2RS task. Due to the size of the OC20 dataset (over 14 million data points in the 200k training split), it is not computationally feasible to train an ensemble of models, making LTAU-FF a particularly attractive alternative to Ensemble for this task. In the IS2RS task, a model is given an initial atomic configuration and is asked to predict the relaxed state, which is a broadly-applicable and extremely valuable task for materials discovery. While some models use the “direct” approach of predicting the relaxed structure directly from the input configuration, an alternative approach (shown to achieve better performance in [69]) is to perform relaxation via energy minimization, which is our approach in this work.

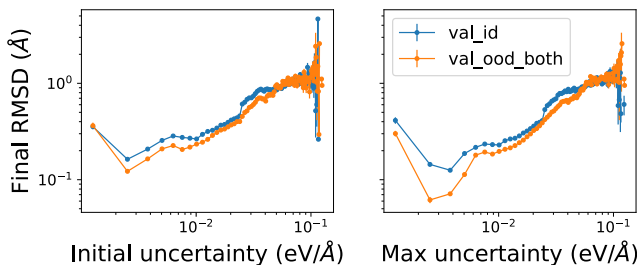


Figure 3: RMSD between atoms of DFT-relaxed and model-relaxed samples from the IS2RS task of OC20, binned by predicted uncertainty. Panels correspond to different choices of snapshots along the relaxation trajectory to use for predicting the final RMSD. The splits identified by [63] as being in-domain (`val_id`) or out-of-domain (`val_ood_both`) are shown in blue or orange, respectively. Distances are averaged within each bin, and error bars correspond to the standard error for each bin. Only the adsorbate and surface atoms were considered in these plots, as is done in [63].

A particularly challenging aspect of predicting errors from a relaxation trajectory is that relatively small errors at any point in the trajectory may drastically alter the predicted relaxed structure by causing the model to relax towards an incorrect local energy minimum. Because of this, in Fig. 3 we consider both the initial uncertainty as well as the maximum uncertainty predicted during energy minimization, both of which show strong correlation with the final root mean-squared displacement (RMSD) of the relaxed structure. Notably, there is significantly more variation in the RMSD at larger uncertainties, reflecting the fact that sufficiently large errors at any point in the simulation can drastically alter the relaxation trajectory. These results motivate the importance of further research into uncertainty propagation methods for molecular simulations, which would benefit greatly from the computational efficiency of LTAU-FF to allow the methods to be applied to large-scale simulations.

4.3 Computational cost

To better understand the computational cost of LTAU-FF relative to other aspects of model evaluation, we ran profiling tests computing the atomic forces and uncertainties for 500 randomly sampled atomic configurations from each test set. These results were obtained using the CPU implementation of FAISS and a TorchScript-compiled NequIP model running on a single NVIDIA V100 GPU. The cost breakdown shown in Table A1 reveals that computing the uncertainty estimates for LTAU-FF occupies about 1% of the walltime for 3BPA and Carbon_GAP_20, or 7% for OC20. This can be compared to the 15-50% for graph construction and 40-80% for the model forward pass.

While LTAU-FF is 10-50 \times cheaper than the cost of a forward pass of the model, Ensemble can be expected to be approximately M \times the cost of the forward pass. Given that ensemble sizes of $5 \leq M \leq 30$ have been observed to be necessary for Ensemble [24, 25], this means that LTAU-FF can be expected to be 2-3 orders of magnitude faster than Ensemble in practice for inference. Furthermore, since LTAU-FF only requires the training trajectory from a single model, it can be easily applied to tasks like the OC20 dataset where it is impractical to train multiple models. Considering that many practical applications of atomistic force fields involve simulating systems with millions or even billions of atoms, and that so-called “universal” interatomic potentials [70, 71] require training to massive datasets, we believe that LTAU-FF will be an essential tool for UQ in this field.

5 Conclusion

In this work, we developed LTAU, a novel UQ method based on the per-sample PDFs of training errors and a distance-based similarity search, and demonstrated its utility in the field of atomistic simulations (LTAU-FF). We outlined how LTAU-FF, which avoids many of the drawbacks of previous ensemble-based UQ methods for atomistic force fields, can be readily applied to any model while introducing only negligible computational overhead and requiring only minor modifications to training software. Finally, we show that the UQ metric produced by LTAU-FF outperforms the gold standard ensemble method on ID data, has promising avenues for detecting OOD data, and can be used as a reliable tool for re-weighting training sets and predicting model failure during simulations.

Further research coupling LTAU with more advanced clustering methods, error propagation techniques, or other modifications that may improve the diversity of the ensemble even more (e.g., alternative loss functions or training regimen) would be particularly welcome contributions. We are also interested in exploring methods beyond those proposed in Section 4.1 for improving the ability of LTAU-FF to detect OOD data and make more accurate predictions on near-OOD data. Finally, we point out that although in this work we only assessed LTAU as applied to atomistic force fields, the mathematical foundations of our method allow it to be applied to any regression task, and we fully intend to explore its use in other machine learning applications in future work.

6 Data and code availability

All training sets can be found at their original sources. The LTAU-FF code and all models developed in this work will be provided upon completion of the peer review of this paper. Code for computing miscalibration areas is available at <https://github.com/uncertainty-toolbox/uncertainty-toolbox/> under the MIT license. Code for training the NequIP models is available at <https://github.com/mir-group/nequip> under the MIT license.

7 Author contributions

Joshua A. Vita: Conceptualization, Methodology, Software, Validation, Formal analysis, Investigation, Data Curation, Writing - Original Draft, Writing - Review & Editing, Visualization. **Amit Samanta:** Methodology, Writing - Review & Editing, Supervision **Fei Zhou:** Methodology, Writing - Review & Editing, Supervision **Vincenzo Lordi:** Methodology, Resources, Writing - Review & Editing, Supervision, Project administration, Funding acquisition.

8 Acknowledgments

This work was performed under the auspices of the U.S. Department of Energy by Lawrence Livermore National Laboratory under Contract DE-AC52-07NA27344, funded by the Laboratory Directed Research and Development Program at LLNL under project tracking code 23-SI-006. The authors would also like to thank Jared Stimac for providing useful discussions on comparing UQ metrics.

References

- [1] Volker L. Deringer, Miguel A. Caro, and Gábor Csányi. Machine learning interatomic potentials as emerging tools for materials science. *Advanced Materials*, 31(46), September 2019. ISSN 1521-4095. doi: 10.1002/adma.201902765. URL <http://dx.doi.org/10.1002/adma.201902765>.
- [2] Tim Mueller, Alberto Hernandez, and Chuhong Wang. Machine learning for interatomic potential models. *The Journal of Chemical Physics*, 152(5), February 2020. ISSN 1089-7690. doi: 10.1063/1.5126336. URL <http://dx.doi.org/10.1063/1.5126336>.
- [3] Y. Mishin. Machine-learning interatomic potentials for materials science. *Acta Materialia*, 214:116980, August 2021. ISSN 1359-6454. doi: 10.1016/j.actamat.2021.116980. URL <http://dx.doi.org/10.1016/j.actamat.2021.116980>.
- [4] Kien Nguyen-Cong, Jonathan T. Willman, Stan G. Moore, Anatoly B. Belonoshko, Rahul Kumar Gayatri, Evan Weinberg, Mitchell A. Wood, Aidan P. Thompson, and Ivan I. Oleynik. Billion atom molecular dynamics simulations of carbon at extreme conditions and experimental time and length scales. In *Proceedings of the International Conference for High Performance Computing, Networking, Storage and Analysis, SC '21*. ACM, November 2021. doi: 10.1145/3458817.3487400. URL <http://dx.doi.org/10.1145/3458817.3487400>.
- [5] Albert Musaelian, Anders Johansson, Simon Batzner, and Boris Kozinsky. Scaling the leading accuracy of deep equivariant models to biomolecular simulations of realistic size, 2023. URL <https://arxiv.org/abs/2304.10061>.

- [6] Albert P. Bartók, Mike C. Payne, Risi Kondor, and Gábor Csányi. Gaussian approximation potentials: The accuracy of quantum mechanics, without the electrons. *Physical Review Letters*, 104(13), April 2010. ISSN 1079-7114. doi: 10.1103/physrevlett.104.136403. URL <http://dx.doi.org/10.1103/PhysRevLett.104.136403>.
- [7] Anders S. Christensen, Lars A. Bratholm, Felix A. Faber, and O. Anatole von Lilienfeld. Fchl revisited: Faster and more accurate quantum machine learning. *The Journal of Chemical Physics*, 152(4), January 2020. ISSN 1089-7690. doi: 10.1063/1.5126701. URL <http://dx.doi.org/10.1063/1.5126701>.
- [8] Alberto Hernandez, Adarsh Balasubramanian, Fenglin Yuan, Simon A. M. Mason, and Tim Mueller. Fast, accurate, and transferable many-body interatomic potentials by symbolic regression. *npj Computational Materials*, 5(1), November 2019. ISSN 2057-3960. doi: 10.1038/s41524-019-0249-1. URL <http://dx.doi.org/10.1038/s41524-019-0249-1>.
- [9] Jörg Behler and Michele Parrinello. Generalized neural-network representation of high-dimensional potential-energy surfaces. *Physical Review Letters*, 98(14), April 2007. ISSN 1079-7114. doi: 10.1103/physrevlett.98.146401. URL <http://dx.doi.org/10.1103/PhysRevLett.98.146401>.
- [10] Sergei Manzhos and Tucker Carrington. Neural network potential energy surfaces for small molecules and reactions. *Chemical Reviews*, 121(16):10187–10217, October 2020. ISSN 1520-6890. doi: 10.1021/acs.chemrev.0c00665. URL <http://dx.doi.org/10.1021/acs.chemrev.0c00665>.
- [11] Simon Batzner, Albert Musaelian, Lixin Sun, Mario Geiger, Jonathan P. Mailoa, Mordechai Kornbluth, Nicola Molinari, Tess E. Smidt, and Boris Kozinsky. E(3)-equivariant graph neural networks for data-efficient and accurate interatomic potentials. *Nature Communications*, 13(1), May 2022. ISSN 2041-1723. doi: 10.1038/s41467-022-29939-5. URL <http://dx.doi.org/10.1038/s41467-022-29939-5>.
- [12] Ilyes Batatia, Dávid Péter Kovács, Gregor N. C. Simm, Christoph Ortner, and Gábor Csányi. Mace: Higher order equivariant message passing neural networks for fast and accurate force fields, 2022. URL <https://arxiv.org/abs/2206.07697>.
- [13] Mingjian Wen and Ellad B. Tadmor. Uncertainty quantification in molecular simulations with dropout neural network potentials. *npj Computational Materials*, 6(1), August 2020. ISSN 2057-3960. doi: 10.1038/s41524-020-00390-8. URL <http://dx.doi.org/10.1038/s41524-020-00390-8>.
- [14] Panagiotis Angelikopoulos, Costas Papadimitriou, and Petros Koumoutsakos. Bayesian uncertainty quantification and propagation in molecular dynamics simulations: A high performance computing framework. *The Journal of Chemical Physics*, 137(14), October 2012. ISSN 1089-7690. doi: 10.1063/1.4757266. URL <http://dx.doi.org/10.1063/1.4757266>.
- [15] Yu Xie, Jonathan Vandermause, Lixin Sun, Andrea Cepellotti, and Boris Kozinsky. Bayesian force fields from active learning for simulation of inter-dimensional transformation of stanene. *npj Computational Materials*, 7(1), March 2021. ISSN 2057-3960. doi: 10.1038/s41524-021-00510-y. URL <http://dx.doi.org/10.1038/s41524-021-00510-y>.
- [16] Albert Zhu, Simon Batzner, Albert Musaelian, and Boris Kozinsky. Fast uncertainty estimates in deep learning interatomic potentials. *The Journal of Chemical Physics*, 158(16), April 2023. ISSN 1089-7690. doi: 10.1063/5.0136574. URL <http://dx.doi.org/10.1063/5.0136574>.
- [17] Balaji Lakshminarayanan, Alexander Pritzel, and Charles Blundell. Simple and scalable predictive uncertainty estimation using deep ensembles, 2016. URL <https://arxiv.org/abs/1612.01474>.
- [18] Xinlei Zhou, Han Liu, Farhad Pourpanah, Tiejong Zeng, and Xizhao Wang. A survey on epistemic (model) uncertainty in supervised learning: Recent advances and applications. *Neuro-computing*, 489:449–465, June 2022. ISSN 0925-2312. doi: 10.1016/j.neucom.2021.10.119. URL <http://dx.doi.org/10.1016/j.neucom.2021.10.119>.

- [19] Jonas Busk, Peter Bjørn Jørgensen, Arghya Bhowmik, Mikkel N Schmidt, Ole Winther, and Tejs Vegge. Calibrated uncertainty for molecular property prediction using ensembles of message passing neural networks. *Machine Learning: Science and Technology*, 3(1):015012, December 2021. ISSN 2632-2153. doi: 10.1088/2632-2153/ac3eb3. URL <http://dx.doi.org/10.1088/2632-2153/AC3EB3>.
- [20] Lior Hirschfeld, Kyle Swanson, Kevin Yang, Regina Barzilay, and Connor W. Coley. Uncertainty quantification using neural networks for molecular property prediction. *Journal of Chemical Information and Modeling*, 60(8):3770–3780, July 2020. ISSN 1549-960X. doi: 10.1021/acs.jcim.0c00502. URL <http://dx.doi.org/10.1021/acs.jcim.0c00502>.
- [21] Shunzhou Wan, Robert C. Sinclair, and Peter V. Coveney. Uncertainty quantification in classical molecular dynamics. *Philosophical Transactions of the Royal Society A: Mathematical, Physical and Engineering Sciences*, 379(2197), March 2021. ISSN 1471-2962. doi: 10.1098/rsta.2020.0082. URL <http://dx.doi.org/10.1098/rsta.2020.0082>.
- [22] Jesús Carrete, Hadrián Montes-Campos, Ralf Wanzenböck, Esther Heid, and Georg K. H. Madsen. Deep ensembles vs committees for uncertainty estimation in neural-network force fields: Comparison and application to active learning. *The Journal of Chemical Physics*, 158(20), May 2023. ISSN 1089-7690. doi: 10.1063/5.0146905. URL <http://dx.doi.org/10.1063/5.0146905>.
- [23] Tom Wollschläger, Nicholas Gao, Bertrand Charpentier, Mohamed Amine Ketata, and Stephan Günnemann. Uncertainty estimation for molecules: Desiderata and methods, 2023. URL <https://arxiv.org/abs/2306.14916>.
- [24] Michael Gastegger, Jörg Behler, and Philipp Marquetand. Machine learning molecular dynamics for the simulation of infrared spectra. *Chemical Science*, 8(10):6924–6935, 2017. ISSN 2041-6539. doi: 10.1039/c7sc02267k. URL <http://dx.doi.org/10.1039/C7SC02267K>.
- [25] Shuaihua Lu, Luca M. Ghiringhelli, Christian Carbogno, Jinlan Wang, and Matthias Scheffler. On the uncertainty estimates of equivariant-neural-network-ensembles interatomic potentials, 2023. URL <https://arxiv.org/abs/2309.00195>.
- [26] Aik Rui Tan, Shingo Urata, Samuel Goldman, Johannes C. B. Dietschreit, and Rafael Gómez-Bombarelli. Single-model uncertainty quantification in neural network potentials does not consistently outperform model ensembles. *npj Computational Materials*, 9(1), December 2023. ISSN 2057-3960. doi: 10.1038/s41524-023-01180-8. URL <http://dx.doi.org/10.1038/s41524-023-01180-8>.
- [27] Leonid Kahle and Federico Zipoli. Quality of uncertainty estimates from neural network potential ensembles. *Physical Review E*, 105(1), January 2022. ISSN 2470-0053. doi: 10.1103/physreve.105.015311. URL <http://dx.doi.org/10.1103/PhysRevE.105.015311>.
- [28] Stanislav Fort, Huiyi Hu, and Balaji Lakshminarayanan. Deep ensembles: A loss landscape perspective, 2019. URL <https://arxiv.org/abs/1912.02757>.
- [29] Romain Egele, Romit Maulik, Krishnan Raghavan, Bethany Lusch, Isabelle Guyon, and Prasanna Balaprakash. Autodeuq: Automated deep ensemble with uncertainty quantification. In *2022 26th International Conference on Pattern Recognition (ICPR)*. IEEE, August 2022. doi: 10.1109/icpr56361.2022.9956231. URL <http://dx.doi.org/10.1109/ICPR56361.2022.9956231>.
- [30] Andrew A. Peterson, Rune Christensen, and Alireza Khorshidi. Addressing uncertainty in atomistic machine learning. *Physical Chemistry Chemical Physics*, 19(18):10978–10985, 2017. ISSN 1463-9084. doi: 10.1039/c7cp00375g. URL <http://dx.doi.org/10.1039/C7CP00375G>.
- [31] Sepp Hochreiter and Jürgen Schmidhuber. Simplifying neural nets by discovering flat minima. *Advances in Neural Information Processing Systems*, 7, 1994.

- [32] Pratik Chaudhari, Anna Choromanska, Stefano Soatto, Yann LeCun, Carlo Baldassi, Christian Borgs, Jennifer Chayes, Levent Sagun, and Riccardo Zecchina. Entropy-SGD: Biasing Gradient Descent Into Wide Valleys. *arXiv:1611.01838*, 2016. URL <http://arxiv.org/abs/1611.01838>.
- [33] Hao Li, Zheng Xu, Gavin Taylor, Christoph Studer, and Tom Goldstein. Visualizing the loss landscape of neural nets, 2017. URL <https://arxiv.org/abs/1712.09913>.
- [34] Stanislav Fort and Adam Scherlis. The goldilocks zone: Towards better understanding of neural network loss landscapes, 2018. URL <https://arxiv.org/abs/1807.02581>.
- [35] Justin Gilmer, Behrooz Ghorbani, Ankush Garg, Sneha Kudugunta, Behnam Neyshabur, David Cardoze, George Dahl, Zachary Nado, and Orhan Firat. A loss curvature perspective on training instability in deep learning, 2021. URL <https://arxiv.org/abs/2110.04369>.
- [36] Stanislav Fort, Gintare Karolina Dziugaite, Mansheej Paul, Sepideh Kharaghani, Daniel M. Roy, and Surya Ganguli. Deep learning versus kernel learning: an empirical study of loss landscape geometry and the time evolution of the neural tangent kernel, 2020. URL <https://arxiv.org/abs/2010.15110>.
- [37] Stanislav Fort, Jie Ren, and Balaji Lakshminarayanan. Exploring the limits of out-of-distribution detection, 2021. URL <https://arxiv.org/abs/2106.03004>.
- [38] Swabha Swayamdipta, Roy Schwartz, Nicholas Lourie, Yizhong Wang, Hannaneh Hajishirzi, Noah A. Smith, and Yejin Choi. Dataset cartography: Mapping and diagnosing datasets with training dynamics, 2020. URL <https://arxiv.org/abs/2009.10795>.
- [39] Geoff Pleiss, Tianyi Zhang, Ethan R. Elenberg, and Kilian Q. Weinberger. Identifying mislabeled data using the area under the margin ranking, 2020. URL <https://arxiv.org/abs/2001.10528>.
- [40] Chirag Agarwal, Daniel D’souza, and Sara Hooker. Estimating example difficulty using variance of gradients, 2020. URL <https://arxiv.org/abs/2008.11600>.
- [41] Mansheej Paul, Surya Ganguli, and Gintare Karolina Dziugaite. Deep learning on a data diet: Finding important examples early in training. 2021. doi: 10.48550/ARXIV.2107.07075. URL <https://arxiv.org/abs/2107.07075>.
- [42] Nabeel Seedat, Jonathan Crabbé, Zhaozhi Qian, and Mihaela van der Schaar. Triage: Characterizing and auditing training data for improved regression, 2023. URL <https://arxiv.org/abs/2310.18970>.
- [43] Mariya Toneva, Alessandro Sordani, Remi Tachet des Combes, Adam Trischler, Yoshua Bengio, and Geoffrey J. Gordon. An empirical study of example forgetting during deep neural network learning, 2018. URL <https://arxiv.org/abs/1812.05159>.
- [44] Baharan Mirzasoleiman, Jeff Bilmes, and Jure Leskovec. Coresets for data-efficient training of machine learning models. 2019. doi: 10.48550/ARXIV.1906.01827. URL <https://arxiv.org/abs/1906.01827>.
- [45] Krishnateja Killamsetty, Durga Sivasubramanian, Ganesh Ramakrishnan, and Rishabh Iyer. Glist: Generalization based data subset selection for efficient and robust learning. 2020. doi: 10.48550/ARXIV.2012.10630. URL <https://arxiv.org/abs/2012.10630>.
- [46] Krishnateja Killamsetty, Durga Sivasubramanian, Ganesh Ramakrishnan, Abir De, and Rishabh Iyer. Grad-match: Gradient matching based data subset selection for efficient deep model training, 2021. URL <https://arxiv.org/abs/2103.00123>.
- [47] Ben Sorscher, Robert Geirhos, Shashank Shekhar, Surya Ganguli, and Ari S. Morcos. Beyond neural scaling laws: beating power law scaling via data pruning, 2022. URL <https://arxiv.org/abs/2206.14486>.
- [48] Vitaly Feldman. Does learning require memorization? a short tale about a long tail, 2019. URL <https://arxiv.org/abs/1906.05271>.

- [49] Vitaly Feldman and Chiyuan Zhang. What neural networks memorize and why: Discovering the long tail via influence estimation, 2020. URL <https://arxiv.org/abs/2008.03703>.
- [50] Kelvin Guu, Albert Webson, Ellie Pavlick, Lucas Dixon, Ian Tenney, and Tolga Bolukbasi. Simfluence: Modeling the influence of individual training examples by simulating training runs, 2023. URL <https://arxiv.org/abs/2303.08114>.
- [51] Garima Pruthi, Frederick Liu, Mukund Sundararajan, and Satyen Kale. Estimating training data influence by tracing gradient descent, 2020. URL <https://arxiv.org/abs/2002.08484>.
- [52] Stephan Rabanser, Anvith Thudi, Kimia Hamidieh, Adam Dziedzic, and Nicolas Papernot. Selective classification via neural network training dynamics, 2022. URL <https://arxiv.org/abs/2205.13532>.
- [53] Ruifeng Liu and Anders Wallqvist. Molecular similarity-based domain applicability metric efficiently identifies out-of-domain compounds. *Journal of Chemical Information and Modeling*, 59(1):181–189, November 2018. ISSN 1549-960X. doi: 10.1021/acs.jcim.8b00597. URL <http://dx.doi.org/10.1021/acs.jcim.8b00597>.
- [54] Moloud Abdar, Farhad Pourpanah, Sadiq Hussain, Dana Rezazadegan, Li Liu, Mohammad Ghavamzadeh, Paul Fieguth, Xiaochun Cao, Abbas Khosravi, U. Rajendra Acharya, Vladimir Makarenkov, and Saeid Nahavandi. A review of uncertainty quantification in deep learning: Techniques, applications and challenges. *Information Fusion*, 76:243–297, December 2021. ISSN 1566-2535. doi: 10.1016/j.inffus.2021.05.008. URL <http://dx.doi.org/10.1016/j.inffus.2021.05.008>.
- [55] Jon Paul Janet, Chenru Duan, Tzuhsiung Yang, Aditya Nandy, and Heather J. Kulik. A quantitative uncertainty metric controls error in neural network-driven chemical discovery. *Chemical Science*, 10(34):7913–7922, 2019. ISSN 2041-6539. doi: 10.1039/c9sc02298h. URL <http://dx.doi.org/10.1039/C9SC02298H>.
- [56] Pascal Pernot. The long road to calibrated prediction uncertainty in computational chemistry. *The Journal of Chemical Physics*, 156(11), March 2022. ISSN 1089-7690. doi: 10.1063/5.0084302. URL <http://dx.doi.org/10.1063/5.0084302>.
- [57] Yuge Hu, Joseph Musielewicz, Zachary W Ulissi, and Andrew J Medford. Robust and scalable uncertainty estimation with conformal prediction for machine-learned interatomic potentials. *Machine Learning: Science and Technology*, 3(4):045028, December 2022. ISSN 2632-2153. doi: 10.1088/2632-2153/aca7b1. URL <http://dx.doi.org/10.1088/2632-2153/aca7b1>.
- [58] Ilyes Batatia, Simon Batzner, Dávid Péter Kovács, Albert Musaelian, Gregor N. C. Simm, Ralf Drautz, Christoph Ortner, Boris Kozinsky, and Gábor Csányi. The design space of e(3)-equivariant atom-centered interatomic potentials, 2022. URL <https://arxiv.org/abs/2205.06643>.
- [59] Kristof T. Schütt, Oliver T. Unke, and Michael Gastegger. Equivariant message passing for the prediction of tensorial properties and molecular spectra, 2021. URL <https://arxiv.org/abs/2102.03150>.
- [60] Patrick Reiser, Marlen Neubert, André Eberhard, Luca Torresi, Chen Zhou, Chen Shao, Housam Metni, Clint van Hoesel, Henrik Schopmans, Timo Sommer, and Pascal Friederich. Graph neural networks for materials science and chemistry. *Communications Materials*, 3(1), November 2022. ISSN 2662-4443. doi: 10.1038/s43246-022-00315-6. URL <http://dx.doi.org/10.1038/s43246-022-00315-6>.
- [61] Dávid Péter Kovács, Cas van der Oord, Jiri Kucera, Alice E. A. Allen, Daniel J. Cole, Christoph Ortner, and Gábor Csányi. Linear atomic cluster expansion force fields for organic molecules: Beyond rmse. *Journal of Chemical Theory and Computation*, 17(12):7696–7711, November 2021. ISSN 1549-9626. doi: 10.1021/acs.jctc.1c00647. URL <http://dx.doi.org/10.1021/acs.jctc.1c00647>.

- [62] Patrick Rowe, Volker L. Deringer, Piero Gasparotto, Gábor Csányi, and Angelos Michaelides. An accurate and transferable machine learning potential for carbon. *The Journal of Chemical Physics*, 153(3), July 2020. ISSN 1089-7690. doi: 10.1063/5.0005084. URL <http://dx.doi.org/10.1063/5.0005084>.
- [63] Lowik Chanussot, Abhishek Das, Siddharth Goyal, Thibaut Lavril, Muhammed Shuaibi, Morgane Riviere, Kevin Tran, Javier Heras-Domingo, Caleb Ho, Weihua Hu, Aini Palizhati, Anuroop Sriram, Brandon Wood, Junwoong Yoon, Devi Parikh, C. Lawrence Zitnick, and Zachary Ulissi. Open catalyst 2020 (oc20) dataset and community challenges. *ACS Catalysis*, 11(10):6059–6072, May 2021. ISSN 2155-5435. doi: 10.1021/acscatal.0c04525. URL <http://dx.doi.org/10.1021/acscatal.0c04525>.
- [64] Zun Wang, Hongfei Wu, Lixin Sun, Xinheng He, Zhirong Liu, Bin Shao, Tong Wang, and Tie-Yan Liu. Improving machine learning force fields for molecular dynamics simulations with fine-grained force metrics. *The Journal of Chemical Physics*, 159(3), July 2023. ISSN 1089-7690. doi: 10.1063/5.0147023. URL <http://dx.doi.org/10.1063/5.0147023>.
- [65] Jeff Johnson, Matthijs Douze, and Hervé Jégou. Billion-scale similarity search with GPUs. *IEEE Transactions on Big Data*, 7(3):535–547, 2019.
- [66] Kevin Tran, Willie Neiswanger, Junwoong Yoon, Qingyang Zhang, Eric Xing, and Zachary W Ulissi. Methods for comparing uncertainty quantifications for material property predictions. *Machine Learning: Science and Technology*, 1(2):025006, May 2020. ISSN 2632-2153. doi: 10.1088/2632-2153/ab7e1a. URL <http://dx.doi.org/10.1088/2632-2153/ab7e1a>.
- [67] Jim Winkens, Rudy Bunel, Abhijit Guha Roy, Robert Stanforth, Vivek Natarajan, Joseph R. Ledsam, Patricia MacWilliams, Pushmeet Kohli, Alan Karthikesalingam, Simon Kohl, Taylan Cemgil, S. M. Ali Eslami, and Olaf Ronneberger. Contrastive training for improved out-of-distribution detection, 2020. URL <https://arxiv.org/abs/2007.05566>.
- [68] Volodymyr Kuleshov, Nathan Fenner, and Stefano Ermon. Accurate uncertainties for deep learning using calibrated regression, 2018. URL <https://arxiv.org/abs/1807.00263>.
- [69] Lowik Chanussot, Abhishek Das, Siddharth Goyal, Thibaut Lavril, Muhammed Shuaibi, Morgane Riviere, Kevin Tran, Javier Heras-Domingo, Caleb Ho, Weihua Hu, Aini Palizhati, Anuroop Sriram, Brandon Wood, Junwoong Yoon, Devi Parikh, C. Lawrence Zitnick, and Zachary Ulissi. Correction to “the open catalyst 2020 (oc20) dataset and community challenges”. *ACS Catalysis*, 11(21):13062–13065, October 2021. ISSN 2155-5435. doi: 10.1021/acscatal.1c04408. URL <http://dx.doi.org/10.1021/acscatal.1c04408>.
- [70] Chi Chen and Shyue Ping Ong. A universal graph deep learning interatomic potential for the periodic table. *Nature Computational Science*, 2(11):718–728, November 2022. ISSN 2662-8457. doi: 10.1038/s43588-022-00349-3. URL <http://dx.doi.org/10.1038/s43588-022-00349-3>.
- [71] Ilyes Batatia, Philipp Benner, Yuan Chiang, Alin M. Elena, Dávid P. Kovács, Janosh Riebesell, Xavier R. Advincula, Mark Asta, Matthew Avaylon, William J. Baldwin, Fabian Berger, Noam Bernstein, Arghya Bhowmik, Samuel M. Blau, Vlad Cărare, James P. Darby, Sandip De, Flaviano Della Pia, Volker L. Deringer, Rokas Elijošius, Zakariya El-Machachi, Fabio Falcioni, Edvin Fako, Andrea C. Ferrari, Annalena Genreith-Schriever, Janine George, Rhys E. A. Goodall, Clare P. Grey, Petr Grigorev, Shuang Han, Will Handley, Hendrik H. Heenen, Kersti Hermansson, Christian Holm, Jad Jaafar, Stephan Hofmann, Konstantin S. Jakob, Hyunwook Jung, Venkat Kapil, Aaron D. Kaplan, Nima Karimitari, James R. Kermode, Namu Kroupa, Jolla Kullgren, Matthew C. Kuner, Domantas Kuryla, Guoda Liepuoniute, Johannes T. Margraf, Ioan-Bogdan Magdău, Angelos Michaelides, J. Harry Moore, Aakash A. Naik, Samuel P. Niblett, Sam Walton Norwood, Niamh O’Neill, Christoph Ortner, Kristin A. Persson, Karsten Reuter, Andrew S. Rosen, Lars L. Schaaf, Christoph Schran, Benjamin X. Shi, Eric Sivonxay, Tamás K. Stenczel, Viktor Svahn, Christopher Sutton, Thomas D. Swinburne, Jules Tilly, Cas van der Oord, Eszter Varga-Umbrich, Tejs Vegge, Martin Vondrák, Yangshuai Wang, William C. Witt, Fabian Zills, and Gábor Csányi. A foundation model for atomistic materials chemistry, 2024. URL <https://arxiv.org/abs/2401.00096>.

- [72] Yu. A. Malkov and D. A. Yashunin. Efficient and robust approximate nearest neighbor search using hierarchical navigable small world graphs, 2016. URL <https://arxiv.org/abs/1603.09320>.
- [73] Albert Musaelian, Simon Batzner, Anders Johansson, Lixin Sun, Cameron J. Owen, Mordechai Kornbluth, and Boris Kozinsky. Learning local equivariant representations for large-scale atomistic dynamics. *Nature Communications*, 14(1), February 2023. ISSN 2041-1723. doi: 10.1038/s41467-023-36329-y. URL <http://dx.doi.org/10.1038/s41467-023-36329-y>.

A Additional details on computational cost

All experiments in this work were performed on a single node of the Sierra supercomputer. Each node has 256 GB of CPU memory, 44 CPU cores, and four NVIDIA V100 GPUs (though only one was used due to a lack of multi-GPU support in the NequIP code). Training a single NequIP model on this architecture required walltimes of approximately 4 hours for the 3BPA dataset and 48 hours for the Carbon_GAP_20 dataset. Training to the 200k split of the S2EF task from OC20, which is a significantly larger dataset, required approximately 500 hours.

Table A1: Computational costs of evaluating model uncertainty for the datasets used in this work. Results were obtained by computing forces and uncertainties for a single NequIP model on a random selection of 500 test samples for each dataset. LTAU-FF used $k = 10$ neighbors and descriptors of dimensionality 32 for all datasets.

Dataset	Train size (# atoms)	Operation	% time
3BPA	13,500	UQ (IndexFlatL2)	1.5
		Graph construction	47.0
		Forward pass	51.4
Carbon_GAP_20	400,275	UQ (IndexHNSWFlat)	1.0
		Graph construction	53.3
		Forward pass	45.4
OC20	14,631,937	UQ (IndexHNSWFlat)	7.3
		Graph construction	14.2
		Forward pass	78.0

B Hyperparameter details

B.1 NequIP

Table B1 outlines some of the most important parameters used for defining the NequIP architecture, the training algorithm, or computing the uncertainty estimates for each dataset. Unless otherwise specified, the recommended settings were used for the NequIP model as provided by <https://github.com/mir-group/nequip/blob/main/configs/full.yaml>. The AMSGrad variant of the Adam optimizer was used with an initial learning rate of 0.005, a weight decay of 0, and the ReduceLROnPlateau scheduler. Full configuration files will be provided upon completion of the peer review of this article.

Table B1: The main hyperparameters used for the NequIP model. r_{\max} is the radial cutoff of the model, num_layers is the number of message passing layers, l_{\max} is the symmetry order of the equivariant features, and M is the ensemble size.

Dataset	r_{\max}	num_layers	l_{\max}	F weight	E weight	Batch size	M
3BPA	5.0	5	3	1000.0	0.0	5	10
Carbon_GAP_20	4.5	4	2	10.0	0.0	1	10
OC20	4.0	2	2	100.0	1.0	4	1

B.2 FAISS

The cost of UQ predictions with LTAU-FF is dictated by the complexity of the similarity search performed by the FAISS package, as well as the size of the training set and the dimensionality of the latent space embeddings used as the atomic descriptors. Depending on these factors, particularly the dataset size, different indexing algorithms (as implemented by FAISS) are recommended. For the Carbon_GAP_20 and OC20 datasets, the approximate neighbor search IndexHNSWFlat index was used as opposed to the exact brute-force approach (IndexFlatL2) used for 3BPA. Additional UQ speedups could be obtained by using the GPU implementation of FAISS, decreasing k , or further refining the parameters of the indexers. For a more thorough discussion of indexing methods and hyperparameter choices, we recommend consulting the FAISS documentation.

While the IndexFlatL2 index is a parameter-free brute force approach, the IndexHNSWFlat index has two primary parameters which strongly affect the cost of the similarity search. The Hierarchical Navigable Small Worlds (HNSW) method [72] is an *approximate* similarity search algorithm which decomposes the search space into a multi-layered graph structure. The key parameters of IndexHNSWFlat are M (the number of neighbor links to add for each point in the graph), $efConstruction$ (the number of neighbors to consider at each layer when inserting into the graph), and $efSearch$ (the number of neighbors to consider at each layer when searching the graph). In this work, we used values of $M=32$, $efConstruction=40$, and $efSearch=16$, which we found to provide a reasonable balance between speed and accuracy. The computational cost of model evaluation using these hyperparameters are shown in Table A1. We emphasize that more thorough analysis of the effects of tuning these hyperparameters would be helpful.

C Dataset details

3BPA

The first dataset used in this work is the 3BPA dataset [61], which has been used previously in the literature for benchmarking extrapolation behaviors of force fields [12, 58, 73]. The 3BPA dataset is a molecular dataset consisting of 500 training configurations taken from molecular dynamics (MD) simulations at a temperature of 300 K, where each configuration has 27 atoms for a total of 13,500 training points. There are additionally three separate test sets sampled using MD simulations at temperatures of 300K, 600K, and 1200K, respectively, where increasing the sampling temperature can be expected to push the simulations to explore OOD regions of the available configuration space of the molecule. For 3BPA the predefined training set was used with no validation set. The dataset can be obtained from <https://pubs.acs.org/doi/10.1021/acs.jctc.1c00647> under the CC BY 4.0 license.

Carbon_GAP_20

In order to better understand how LTAU-FF performs on a more challenging dataset, we also used the Carbon_GAP_20 dataset [62], which was originally intended to be used for fitting a model capable of accurately describing a broad range of carbon phases. The Carbon_GAP_20 dataset includes a training set of 6,088 configurations (400,275 atoms), as well as a larger superset containing 17,525 configurations (1,345,246 atoms) which we used for testing. The training and test sets are comprised of an extremely diverse range of phases, including bulk crystals, amorphous carbon, graphene, graphite, fullerene, nanotubes, liquids, surfaces, defected configurations, and other rare allotropes obtained through random structure search or extracted from the literature. Particularly valuable are the labels provided by the authors of the Carbon_GAP_20 dataset for defining conceptually similar clusters over the atomic configurations in the dataset. Although in our analysis we observed a number of mislabeled configurations, the provided groupings are still extremely useful for understanding how models and methods perform across different subsets of the data. A breakdown of the number of atoms in each group in the training set is provided in Table C1. A more thorough description of the dataset can be found in [62]. For Carbon_GAP_20 a random 90–10 training–validation split was used. The dataset can be obtained from <https://www.repository.cam.ac.uk/handle/1810/307452> under the CC BY 4.0 license.

OC20

As a practical application, we also train a model to the S2EF task of the OC20 dataset [63] then test how well the UQ estimate provided by LTAU-FF predicted performance on the ISR2S task. Specifically, we trained to the 200k split (14,631,937 atoms) of the S2EF task, and tested on the `val_id` and `val_ood_both` splits of the ISR2S task. The OC20 dataset includes a wide range of catalysts comprised of various materials, surfaces, and adsorbates. Importantly, the data includes labels for each atom identifying them as an “adsorbate” atom (part of the adsorbing molecule), a “surface” atom (the top few layers of the material), or a “bulk” atom (everything in the material that is not part of the surface). For OC20 the predefined S2EF training set and ISR2S validation sets were used. The dataset can be obtained from <https://fair-chem.github.io/core/datasets/oc20.html> under the MIT license.

Table C1: Number of atomic configurations and atoms within each group of the Carbon_GAP_20 training set.

config_type group	# configurations	# atoms
Amorphous_Bulk	3,053	200,470
Amorphous_Surfaces	20	2,648
Crystalline_Bulk	78	368
Crystalline_RSS	483	8,554
Defects	530	70,022
Diamond	164	1,360
Dimer	26	52
Fullerenes	272	11,782
Graphene	2	400
Graphite	185	6,344
Graphite_Layer_Sep	7	700
LD_iter1	80	14,048
Liquid	6	1,296
Liquid_Interface	17	3,672
Nanotubes	138	4,976
SACADA	755	24,503
Surfaces	271	49,079
Total	6,088	400,275

D Out-of-domain detection

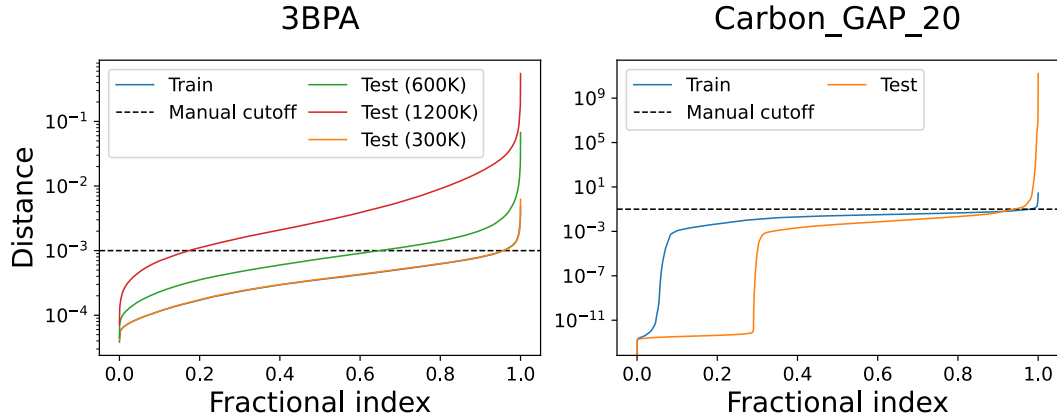


Figure D1: Distributions of first nearest-neighbor distances in the train/test sets of 3BPA and Carbon_GAP_20. The data points are sorted by distance to improve visibility. Each train/test set is plotted as a different color; the 3BPA 300K test data almost exact overlaps the 3BPA train data. Cutoffs (dashed black lines) can be chosen *ad hoc* to identify OOD data where LTAU-FF may begin to suffer from the drawbacks of distance-based UQ metrics discussed in Section 2.2. Fig. D2 and Fig. D3 show that data classified as being OOD roughly corresponds to the points where LTAU-FF fails to accurately predict the true force errors.

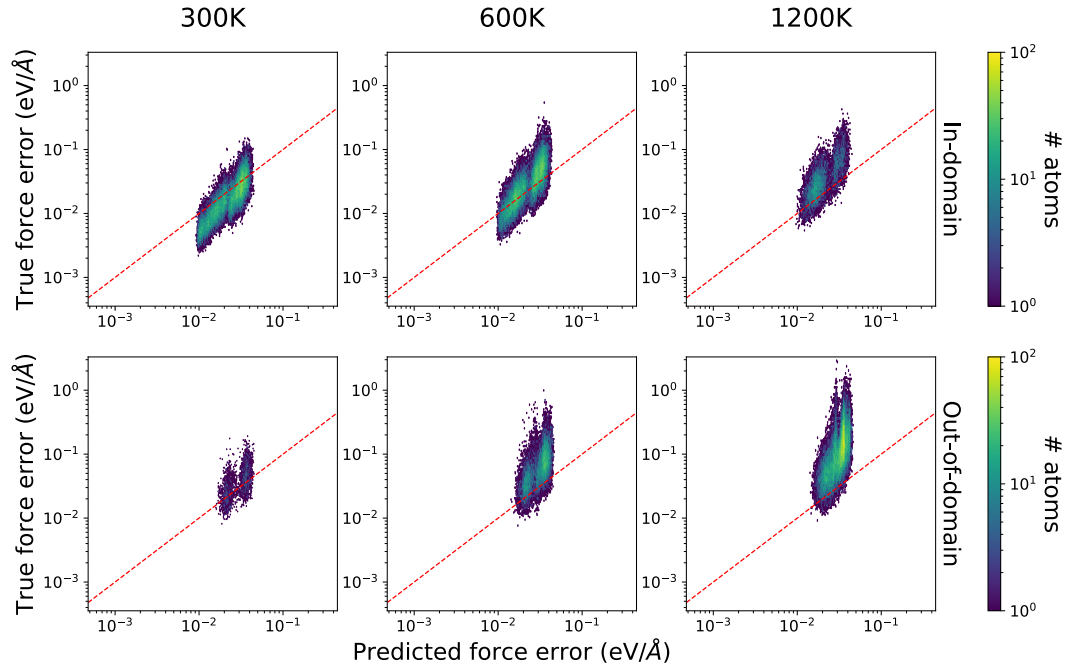


Figure D2: A version of Fig. 1a where the 3BPA test data is split into ID and OOD data based on the manual cutoffs defined in Fig. D1.

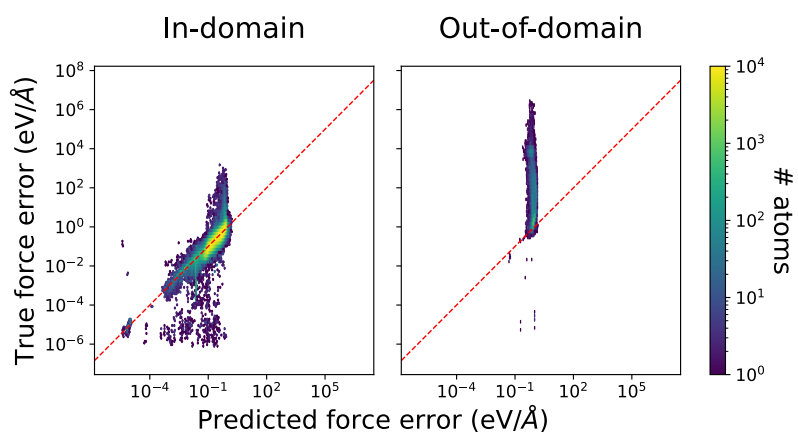


Figure D3: A version of Fig. 2a where the Carbon_GAP_20 test data is split into ID and OOD data based on the manual cutoffs defined in Fig. D1.

E Dataset re-weighting

In [38], a model is said to be “confident” in its prediction for a given point if the point has a high probability of being correctly predicted (i.e., high average Softmax activation) throughout the course of training. Since regression tasks do not normally have a Softmax output layer and there is no binary notion of “correctness”, we instead chose to define the “difficulty” of a sample as the likelihood (over the course of training) of it having errors above the final mean absolute training error (MAE). Since LTAU-FF already requires recording the PDFs of per-sample errors, this difficulty metric can be easily computed.

In the case of the “up-weight hard” weighting scheme in Fig. E1, atom i was given a weight in the loss function of $w_i = \exp[\lambda(1 - d_i)]$, where $d_i := P(\epsilon_i < \text{MAE})$. In the “up-weight easy” scheme, the weight was given as $w_i = \exp(\lambda d_i)$. Values of λ were determined *ad hoc*, and set to 2.0 and 4.5 for the up-weight easy and hard schemes, respectively.

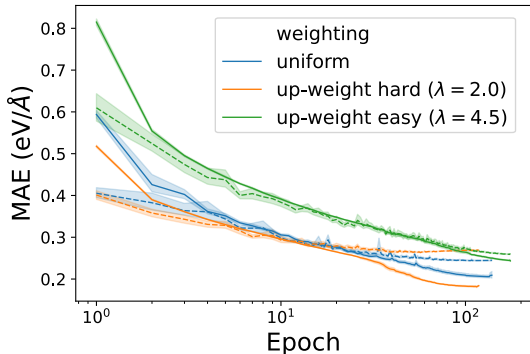


Figure E1: Training (solid lines) and validation (dashed lines) curves for ensembles of 10 models trained to the Carbon_GAP_20 dataset with different weighting schemes. A random 90:10 training:validation split was used, where all runs used the exact same split. Shaded bands denote the 95% confidence intervals computed across the 10 runs for each weighting scheme.

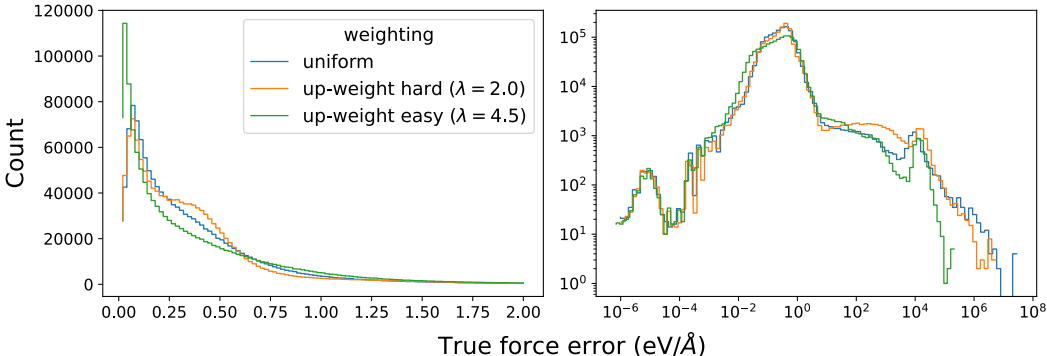


Figure E2: Distributions of test errors on the Carbon_GAP_20 dataset for the three weighting schemes. In panel **a**, the range of the x-axis has been clipped to a maximum value of 2.0 eV/Å in order to improve visualization by removing a small number (3-4%) of points with abnormally large errors. In panel **b**, the full distributions are shown on a log-scale. The average test error for all weighting schemes after removing values larger than 2.0 eV/Å, was around 0.35 eV/Å. However, when including all data from panel **b**, the “up-weight easy” scheme had an MAE of 47eV/Å, which was an order of magnitude lower than the other two schemes.